

Polymer nano-droplets forming liquid bridges in chemically structured slit pores: A computer simulation

Jacqueline Yaneva¹, Andrey Milchev^{1,2}, and Kurt Binder²

¹ Institute for Physical Chemistry, Bulgarian Academy of Sciences, 1113 Sofia, Bulgaria

² Institut für Physik, Johannes-Gutenberg-Universität Mainz, 55099 Mainz, Germany

Using a coarse-grained bead-spring model of flexible polymer chains, the structure of a polymeric nanodroplet adsorbed on a chemically decorated flat wall is investigated by means of Molecular Dynamics simulation. We consider sessile drops on a lyophilic (attractive for the monomers) region of circular shape with radius R_D while the remaining part of the substrate is lyophobic. The variation of the droplet shape, including its contact angle, with R_D is studied, and the density profiles across these droplets also are obtained.

In addition, the interaction of droplets adsorbed on two walls forming a slit pore with two lyophilic circular regions just opposite of one another is investigated, paying attention to the formation of a *liquid bridge* between both walls. A central result of our study is the measurement of the force between the two substrate walls at varying wall separation as well as the kinetics of droplet merging. Our results are compared to various phenomenological theories developed for liquid droplets of mesoscopic rather than nanoscopic size.

1. Introduction

In the context of the emerging technology of microscale processing the use of surface substrates with micropatterns has become increasingly important for microfluidics applications. Chemically structured surfaces that exhibit lateral patterns of varying wettability can be produced by techniques such as photolithography^{1,2}, microcontact printing³⁻⁵, vapor deposition through grids⁶, domain formation in Langmuir-Blodgett monolayers^{7,8}, electrophoretic colloid assembly⁹, lithography with colloid monolayers¹⁰, microphase separation in diblock copolymer films¹¹, etc. For patterned surfaces in the micrometer range, on which liquid droplets or thin liquid films are adsorbed, fascinating wetting morphologies have been predicted¹²⁻¹⁹ (including “morphological wetting transitions”^{12,16,17}) and observed⁶. Liquid bridges between droplets at walls are also of interest in the context of forces between droplets (or bubbles, respectively)^{20,21}, long range forces between colloidal particles^{22,23}, etc. The theoretical treatments mostly apply phenomenological quasi-macroscopic concepts (in terms of interfacial tensions, contact angles,^{24,25} etc.); but for droplets on the micrometer scale the lack of knowledge on the line tension²⁵⁻³⁶ is a serious drawback already, and the understanding of the density distribution of the droplet near the contact line is a difficult problem^{34,35}. The present drive towards nanoscale technology creates also more interest in droplets on the nanometer scale, and in fact some of the techniques mentioned above are well suited to create surface patterns on the nanoscale^{10,11}. Although sometimes macroscopic concepts do allow reasonable predictions down to the nanoscale³⁷⁻⁴⁰, there is no guarantee that the phenomenological theories are quantitatively accurate for bridge formation between polymer nanodroplets. We study this problem here by Molecular-Dynamics simulation, to complement existing knowledge on the problem by insight on a molecular level.

In the next section we shall present our model, which has been used successfully in previous work to study static and dynamic properties of polymers in the bulk and at surfaces^{37-39,41-47}. In section 3 we shall present our simulation results on droplets on single walls, as well as on the structure of liquid bridges in slit pores of varying width. Section 4 is devoted to a discussion of dynamic aspects of bridge formation, while Section 5 summarizes some conclusions.

2. Some comments on the model and the simulation technique

We employ a coarse-grained off-lattice model of polymer chains, where each chain consists of $N = 32$ effective monomers, which are connected by anharmonic springs. These effective bonds are thought to represent groups of a few successive chemical monomers along the chain, and therefore inclusion of torsional potentials and even bond-bending potentials is not considered. The springs are described by the finitely extensible nonlinear elastic (FENE) potential

$$U_{FENE}(\ell) = -\frac{K}{2}R^2\ln\left[1 - \frac{(\ell - \ell_0)^2}{R^2}\right], \quad (1)$$

ℓ being the bond length, which can vary in between ℓ_{\min} and ℓ_{\max} , and thus the equilibrium value ℓ_0 for which $U_{FENE}(\ell_0) = 0$, and $R = \ell_{\max} - \ell_0 = \ell_0 - \ell_{\min}$. The spring constant K is taken as

in previous work $K/k_B T = 40$, and we again choose $\ell_{\max} = 1$ as our unit of length, with $R = 0.3$ (hence $\ell_0 = 0.7$, $\ell_{\min} = 0.4$)^{41–47}.

Between the effective monomers a Morse potential acts,

$$U_M(r) = \epsilon_M \exp[-2\alpha(r - r_{\min})] - 2 \exp[-\alpha(r - r_{\min})], \quad (2)$$

r being the distance between the beads, and the parameters are chosen as $r_{\min} = 0.8$, $\epsilon_M = 1$ and $\alpha = 24$. Owing to the large value of α , $U_M(r)$ decays to zero very rapidly for $r > r_{\min}$, and is completely negligible for $r > 1$. This choice of parameters is useful, particularly for Monte Carlo simulations, since it allows the use of a very efficient link-cell algorithm⁴¹. The Theta-temperature for this model is⁴³ $k_B \Theta \approx 0.62$. We hence choose in the following a temperature $k_B T = 0.49$, where at zero pressure the system already is in the state of a dense melt, and to a very good approximation the gas density is zero for $N = 32$. Thus from a polymer droplet at a surface no chains evaporate into the surrounding gas.

The adsorbing walls are treated as perfectly flat and structureless; in particular, no atomic corrugation of the walls is considered. The interactions between the effective monomers and the walls are represented by a Lennard-Jones potential, integrated over a (semi-infinite) substrate³⁹

$$U_{\text{wall}}(z) = 4\pi\epsilon_w \left[\frac{1}{45} \left(\frac{\sigma_{\text{wall}}}{z} \right)^9 - \frac{1}{6} \left(\frac{\sigma_{\text{wall}}}{z} \right)^3 \right], \quad (3)$$

where we choose parameters $\sigma_{\text{wall}} = 1$, $\epsilon_w = 0.20$ in the lyophilic part of the substrate, while in the lyophobic area $\epsilon_w = 0.05$ is chosen. Typically, the lyophilic area is a circle of radius R_D , with $3 \leq R_D \leq 15$. The total lateral linear dimensions of the simulation box is chosen 64×64 , so that (for a total number of $\mathcal{N} = 128$ chains in the polymer droplet) it never can happen that a droplet interacts with its images generated by the periodic boundary condition. For a study of single droplets, the linear dimensions in the perpendicular direction is $L = 32$, and the top wall of the box is taken purely repulsive (omitting the attractive term from Eq.(3), and choosing also $\epsilon_w = 0.20$). For our study of slit pores, we choose $5 \leq L \leq 22$, and the potentials from both walls are chosen exactly of the same type.

The initial preparation of droplets in equilibrium is done by Monte Carlo methods, applying the Velocity-Verlet algorithm and keeping the temperature constant by the Nosé-Hoover thermostat⁴⁸. In the case of bridging droplets, however, we resort to a Langevin thermostat⁴⁹ which provides greater stability of the algorithm for small separation between the solid planes. For more details on our Molecular Dynamics algorithm, we refer the reader to³⁹. Here we only note that due to the steep variation of the Morse potential a very small integration time step needs to be used, $\delta t = 0.0009$ MD time units, and typically runs over 1.1 million time steps were carried out.

It is certainly useful to translate the time units [t.u.], used in our simulation, into seconds by mapping our model results to laboratory data. A typical substance used in numerous experiments on wetting is, for example, the PDMS (polydimethylsiloxane) melt $(C_2H_6OSi)_n$. In ellipsometric experiments on droplet spreading⁵⁰ one has measured a diffusion coefficient $\mathcal{D}_{diff} \approx 3.3 \times 10^{-10} m^2/s$ for chain lengths $N = 10$, and $\mathcal{D}_{diff} \approx 0.3 \times 10^{-10} m^2/s$ for $N = 20$. These data can be compared to our measurements of precursor diffusion³⁹ in spreading droplets which yield $\mathcal{D}_{diff}^{sim} \approx 0.11 \ell_0^2/t.u.$ in a melt of chains with $N = 32$. Bearing in mind that the bond length in PDMS is⁵¹ $\approx 1.59 \text{ \AA}$, and assuming that, say, three chemical units form a persistent length of $\approx 4 \text{ \AA}$, one obtains for the simulation time unit $1t.u. \approx 0.5ns$ as a rough estimate.

3. Polymer nanodroplets on chemically structured walls: static properties

As discussed in our previous work on droplets adsorbed on flat walls without any chemical structuring on the substrate, the average density distribution $\rho(R, Z)$ is a function of two coordinates, the distance Z from the substrate (note that we orient the z-axis perpendicular to the surface and the origin of the coordinate system is the projection of the center of mass of the droplet on the substrate plane $z = 0$), and the distance R from the z-axis. While individual configurations of the droplet due to statistical fluctuations depend on the angle ψ relative to the x-axis as well³⁷, the average density distribution must have rotation symmetry around the z-axis^{37–39}. When we create a chemical structure on the surface such that the constant ϵ_w describing the wall potential $U_{\text{wall}}(Z)$ in Eq. (3) has one value $\epsilon_w = 0.2$ for $0 < R < R_D$ and a smaller value $\epsilon_w = 0.05$ outside this circle whereby the symmetry axis of the droplet coincides with the axis perpendicular to the midpoint of this lyophilic circle, of course. Therefore it is meaningful to record density profiles $\rho(R, Z)$ of the same type to characterize the average droplet density profile as in our previous work. Fig. 1 shows a few representative examples. While for $R_D = 15$ the droplet sits fully inside the lyophilic circle and hence hardly differs from a droplet on an infinitely extended lyophilic surface, for $R_D \leq 12$ the droplet always extends over the full range of the lyophilic region. One thus can see that the shape of the adsorbed droplet changes when the radius R_D of the lyophilic domain decreases. As expected, the contact angle then varies continuously with R_D , due to the interaction of the contact line and the boundary between the lyophilic and lyophobic regions at the substrate, and is no longer

identical to the contact angle that applies for an infinitely extended flat lyophilic substrate (this contact angle is determined, for very large droplets, in terms of the polymer-wall and polymer-gas interfacial energies, through the Young equation^{24,25} while for not so large droplets also a correction due to the line tension^{35,36} needs to be taken into account^{37,52}). As discussed in our earlier work³⁷, for nanodroplets considered here, some ambiguity in the definition of the contact-angle for these nanodroplets is inevitable. We follow the earlier work³⁷⁻³⁹, fitting a straight line to the density contour $\rho(Z, R) = 1$ in the regime $2 \leq Z \leq 4$, disregarding the slight curvature of this contour in that region. Fig. 2 presents a plot of the resulting variation, showing that $\cos(\theta) \approx \text{const}$ for $R_D \geq 12$, while $\cos(\theta) < 0$ for $R_D < 9$. Comparing the density profiles shown in the insert of Fig. 2 with those of Fig. 1 one sees that indeed for $R_D > 12$ the droplet shape in Fig. 1 is the same as that for a homogeneous surface with $\epsilon_w = 0.2$. Qualitatively, the behavior seen in Figs. 1,2 nicely corresponds to the theoretical predictions of Lipowsky et al.¹²⁻¹⁸. When R_D gets very small, the droplet shape gradually approaches the shape that a droplet takes on a uniformly lyophobic substrate surfaces, as the comparison of the droplet profile for $R_D = 3$ in Fig. 1 and the droplet profile for $\epsilon_w = 0.05$ in Fig. 2 shows.

We next study the behavior of a slit pore of width L , where both walls exhibit a lyophilic domain of radius R_D exactly opposite to each other. When L is large enough, in equilibrium (for a fixed total number \mathcal{N} of chains) we expect that droplets containing $\mathcal{N}/2$ chains each (assuming \mathcal{N} is an even integer) will be adsorbed exactly opposite to each other. However, when the distance L between the plates gets smaller, the two droplets start to interact, and a liquid bridge between both walls can form. This formation of liquid bridges by variation of L is illustrated in Fig. 3, choosing $R_D = 14$ and $\mathcal{N}/2 = 128$, so that the single non-bridging droplets on the separated walls are exactly equivalent to the situation considered in Figs. 1, 2. One can see that for $L = 22$ the droplets are still separated and identical in shape to those seen in Fig. 1 for $12 \leq R_D \leq 15$. For $L \leq 19$, however, bridge formation has occurred. One can clearly see the change of the bridge morphology with decreasing distance L between the two walls. When the separated droplets touch each other, they form an “in-bridge” (i.e., the curvature of the bridge surface is concave) which is typical for liquids wetting the substrate. This catenoid shape is displayed for the profiles when the pore width is $L = 17, 15$, or 13 , respectively. On further decrease of L , the shape of the liquid bridge becomes perfectly cylindrical (the shapes for $L = 10$ and $L = 9$ are close to this shape), while for still smaller slit pore widths L (such as $L = 6$ and $L = 5$) the shape is that of an “out bridge”, with a convex curvature of the bridge surface, i.e. a barrel-like shape. This shape is typical for lyophobic substrates, as experienced here by those monomers of the polymer droplet whose coordinates $R(X, Y)$ exceed the radius R_D of the hydrophilic domain. Again the behavior in Fig. 3 is very nicely consistent with the behavior as predicted by the theory for quasi-macroscopic droplets¹²⁻¹⁹, and hence we again find that these phenomenological concepts due to Lipowsky et al.¹²⁻¹⁸ work qualitatively down to the nanoscopic scale.

In view of the fact that there is some ambiguity in the precise numerical estimation of the contact angle of nanodroplets, as mentioned above, it is of significant interest to estimate additional properties quantitatively, which could be compared to analytical theories on this problem. Such properties are the base radius R_{lat} of the droplet (Fig.4) or liquid bridge (Fig.5), the height of the droplet H (Fig.4), and the midheight radius $R_{\text{lat}}(Z = H/2)$ of the droplet (Fig. 4) or of a liquid bridge $R_{\text{lat}}(Z = L/2)$, (Fig. 5), respectively. Figs. 4,5 demonstrate that these quantities can be measured with relatively small statistical errors in our simulations. From such data it also is evident that a pronounced change in the behavior occurs at $R_D \approx 8.5$ (Fig. 4). For a macroscopic sessile droplet (satisfying the Young equation with the contact angle θ and having a sphere-cap shape) we simply would have the relations in terms of the sphere radius r

$$R_{\text{lat}} = r \sin(\theta), \quad H = r(1 - \cos(\theta)), \quad (4)$$

and hence

$$H/R_{\text{lat}} = (1 - \cos(\theta))/\sin(\theta) \approx \theta/2, \quad \theta \rightarrow 0. \quad (5)$$

Indeed this relation is roughly fulfilled for our model.

It also is of interest to calculate the pressure in the liquid bridge, using the virial formula^{46,53}. Fig.(6) shows that the pressure is positive for the smallest distances between the plates ($L \leq 6$) only, while for larger distances the pressure is negative. This observation already indicates that this situation is unfavorable, if we would not enforce the distance L between the plates as given parameter, such distances would not occur if the walls could freely move against each other. This fact is very clearly borne out when we compute the normal force between the walls (Fig. 7). Of course, for large distances L for which two separate droplets occur on each wall that do not yet touch the force is zero, while for bridging droplets an attractive force arises, and only for very small L , where the bridge is squeezed into the lyophobic part, the force becomes repulsive (Fig. 7). The force goes through zero at $L \approx 6$. Since it has been shown¹⁹ that for the underlying *catenoid* geometry a closed analytical expression for the surface area dependence on the wall separation L does not exist, we tentatively use a relation proposed by Swain and Lipowsky¹⁴ for the bridge between a single pair of opposing lyophilic stripes. The corresponding contact angle θ^* can be calculated then

from $\theta^* = -\tan^{-1}(2R_D/L) \approx 100^\circ$ and agrees with our observations. As expected, this contact angle exceeds $\pi/2$. The strongest attractive force actually does occur near $L \approx 10$, where the angle is $\pi/2$. For $L > 12$ an almost linear decrease of the force sets in, before it discontinuously jumps to zero for $L = 22$.

It is interesting to note that very long range attractive forces have been experimentally detected in AFM measurements of forces between a polystyrene sphere and liquid interfaces^{22,23}, showing a *linear* variation with distance on the scale of 30 nm. Unlike such experiments, in our simulation an electrostatic origin of such long range forces is excluded by construction of our model. The force seen in Fig. 7 is entirely due to the interplay of the various interfacial interactions that control the shape of the liquid bridge. One should also point out that both the course of the bridging force against inter-plate distance L as well as the particular bridge configurations corresponding to various parts of the force distance curve closely match some recent results¹⁹ on classical structureless droplets obtained by two different surface minimization techniques.

4. Dynamic aspects of bridge formation

For $L = 21.5$ one can observe initial states where the two substrates still carry separate droplets, but the wings of their density distributions already overlap, and this interaction between the two droplets starts a merging process which leads to the formation of a liquid bridge. Figs. (8) and (9) analyze the dynamical aspects of this merging process of the two droplets in more detail. One can see that the formation of the liquid bridge is a very slow process, it is clearly diffusion-controlled, there is no evidence of faster hydrodynamic mechanisms. The radius of the midpoint of the bridge seems to grow towards its equilibrium value over a transient period of time according to a $t^{1/4}$ law. This behavior is reminiscent of the growth law with which an interfacial profile between coexisting phases approaches equilibrium⁵⁴.

5. Concluding discussion

In the present work, we have presented Molecular Dynamics simulations addressing the shape of a droplet adsorbed on a spherical lyophilic domain on an otherwise lyophobic flat substrate surface, and the formation of liquid bridges between two such surfaces. Also the forces between these surfaces caused by such liquid bridges have been measured, and the kinetics of the merging of two such droplets into one bridge has been studied.

According to the predictions of Lipowsky et al.^{12–18} one should expect for large enough domain radius R_D that the contact angle θ of the droplet is constant ($\theta = \theta_{\text{phil}}$, the “lyophilic” value, with $\cos \theta_{\text{phil}} \approx 0.57$ in our case, see inset of Fig. 2), until the radius R_{lat} of the droplet matches R_D . For our choice of parameters, this happens for $R_D = R_D^{\text{phil}} \approx 12$. For $R_D < R_D^{\text{phil}}$, one expects that θ should increase such that $R_{\text{lat}} = R_D$ is always maintained, until θ reaches the value of the lyophobic part of the substrate surface, $\theta = \theta_{\text{phob}}$, for $R_D = R_D^{\text{phob}}$, with $\cos \theta_{\text{phob}} \approx -0.6$ in our case. In fact, Fig. 4 nicely verifies the linear variation $R_{\text{lat}} = R_D$ quantitatively up to about $R_D \approx 9$, while for $9 < R_D < R_D^{\text{phil}}$ the further increase of R_{lat} with R_D is slower, and the saturation value of R_{lat} , reached for $R \geq R_D^{\text{phil}}$, is in fact smaller than expected, namely only around $R_{\text{lat}}^{\text{max}} \approx 10$. Of course, some quantitative deviations of our results from the predictions of Lipowsky et al.^{12–18} must be expected, since the latter predictions are asymptotically valid for very large, almost macroscopic, droplets, while our simulations concern nanodroplets, and hence there are no sharp transitions possible when R_D is varied: so Fig. 2 does not show a sharp kink of the curve $\cos(\theta)$ vs. R_D at $R_D = R_D^{\text{phil}}$ but rather a rounded crossover, and also at $R_D = R_D^{\text{phob}}$ only a very smooth variation is seen (in fact, R_D^{phob} is of order unity in our case, and hence cannot be even uniquely identified from our data). Clearly, it would be interesting to analyze the amount of rounding of these “transitions” at $\theta = \theta_{\text{phil}}$ and $\theta = \theta_{\text{phob}}$ theoretically, and to repeat our simulations for larger droplets (and correspondingly chosen larger values of R_D) to see the extent to which these transitions become sharper, but all such extensions of our work would present major difficulties and hence have not been attempted.

We also note that the theory implies that the shape of the droplet should be a sphere cap throughout. In particular, since the volume V of the droplet is constant, we should have

$$V = \frac{\pi H}{6}(3R_{\text{lat}}^2 + H^2) = \text{const} \quad (6)$$

and combining this equation with the geometrical relations for the contact angle, Eqs. (4), (5), in principle the variation of $\cos(\theta)$ with R_D in the regime $R_D^{\text{phob}} < R_D < R_D^{\text{phil}}$ can be explicitly predicted. Noting from Fig. 4 that for $R_D > R_D^{\text{phil}}$ we have $R_{\text{lat}} \approx 10$, $H \approx 7.5$, one obtains

$V \approx 1400$. However, for $R_D \approx 7$ where $R_{\text{lat}} \approx 6.8$, $H \approx 9.3$ (Fig. 4) we find that Eq. (6) would yield only $V \approx 1100$, and for $R_D \approx 5$, where $R_{\text{lat}} \approx 5$, $H \approx 11$ we would get $V \approx 1130$, while for $R_D = R_{\text{lat}} = 3$ where $H \approx 13$ we find $V \approx 1330$. Thus, the geometrical relations on the basis of the sphere cap picture are not verified accurately in our case. This problem is related to the fact that the linear increase of R_{lat} with R_D does not continue all the way to $R_{\text{lat}} = R_D^{\text{phil}} \approx 12$ but R_{lat} is significantly too small for $R_D > 9$. On the other hand, the discrepancies found are not dramatic either, they do not exceed 10-15%, in spite of the nanoscopic size of the droplets. One needs also to consider the fact that this small size leads also to substantial errors and ambiguities when one tries to read off R_{lat} and H from the data. In view of all these problems, the agreement between the simulations and the theoretical descriptions certainly is satisfactory.

Acknowledgments: This research was supported in part by the Deutsche Forschungsgemeinschaft (DFG) under grant number 436 BUL 113/130/2-1.

FIG. 1. Contour diagrams representing the density profiles $\rho(Z, R(X, Y)) = \nu\Delta\rho$, $\nu = 1, 2, \dots, 11$, $\Delta\rho = 0.2$, in the (Z, R) plane, for a droplet containing 128 chains with 32 monomers each, at a temperature $k_B T = 0.49$. The droplet is in contact with an ideally flat lyophobic substrate (represented by the thick grey line in the bottom) decorated with one lyophilic circle of radius R_D (the thick black line in the bottom). The adsorption strengths of the lyophobic wall is $\epsilon_w = 0.05$, while for the lyophilic circle it is $\epsilon_w = 0.2$. Profiles are shown for $R_D = 15, 12, 9, 7, 5$ and 3, respectively. These profiles are obtained by averaging over 10 runs of $2.1 \cdot 10^6$ integration steps each. One MD time step is $\delta t = 0.0009$ MD time units.

FIG. 2. Cosine of the contact angle θ plotted versus the radius R_D of the lyophilic domain, for droplets containing $\mathcal{N} = 128$ chains with $N = 32$ monomers each, at $k_B T = 0.49$. The inset shows the dependence of the contact angle of the droplet at an infinitely extended homogeneous substrate (as considered in Refs.^{37–39}) on the strength ϵ_w of the wall potential. The two contour diagrams in the inset represent the density profiles $\rho(Z, R(X, Y)) = \nu\Delta\rho$, $\nu = 1, 2, \dots, 11$ in the (Z, R) plane of a droplet for the two different adsorption strengths relevant for the present paper, namely for $\epsilon_w = 0.05$ (the value used to model the lyophobic region of the wall) and for $\epsilon_w = 0.2$ (the value used for the lyophilic domain on the surface).

FIG. 3. Contour diagrams representing the density profiles $\rho(Z, R(X, Y)) = \nu\Delta\rho$, $\nu = 1, 2, \dots, 11$ ($\Delta\rho = 0.2$) in the (Z, R) plane for two droplets adsorbed on opposite walls ($L = 22$) or a liquid bridge between the walls ($L = 19, 17, 15, 13, 10, 9, 6, 5$) respectively. The simulated system contains 256 chains with 32 monomers each, the temperature is chosen as $k_B T = 0.49$, and the walls are ideally flat and lyophobic, with an adsorption strength $\epsilon_w = 0.05$, except for a lyophilic circle of radius $R_D = 14$ (with adsorption strength $\epsilon_w = 0.2$). The lyophilic parts of the adsorbing surface are shown by thick black bars, the lyophobic parts by thick grey bars. The profiles are averaged over 18 runs of $1.05 \cdot 10^6$ MD steps.

FIG. 4. Variation of the base radius R_{lat} (circles), the height H (squares) and the midheight radius $R_{\text{lat}}(Z = H/2)$ (diamonds) of a droplet adsorbed on a single circular lyophilic domain of radius R_D plotted vs. R_D at $k_B T = 0.49$. The droplet contains 128 chains with 32 monomers each. The strength of the adsorption potential is $\epsilon_w = 0.2$ inside the lyophilic domain and $\epsilon_w = 0.05$ outside of it. The radii and the height are measured from density profile contour diagrams (taking the contour at midpoint density, $\rho = 1$) averaged over 10 runs of $2.1 \cdot 10^6$ integration steps each. R_{lat} is taken as the maximum lateral extension of the contour (it occurs roughly at $Z = 1.5$). The error bars are obtained by estimating the radii from every single run.

FIG. 5. Variation of the base radius R_{lat} (circles) and the midheight radius $R_{\text{lat}}(Z = L/2)$ (squares) for the liquid bridges of Fig. 3 (for further explanations see the caption of Fig. 4). A log-log plot of $R_{\text{lat}}(Z = L/2)$ vs L (see inset) reveals a power-law relationship $R_{\text{lat}} \propto L^{-0.72}$.

FIG. 6. The pressure in a liquid bridge connecting two flat substrates is plotted against the distance L between the walls. The total pressure is shown by filled circles. Open diamonds show the contribution to the pressure that comes from the wall-monomer interactions, while the open squares show the contribution to the pressure from the monomer-monomer interaction and the kinetic part.

FIG. 7. The normal force acting between two substrates with a bridging droplet plotted versus the distance L . The insets show contour diagrams of the density profiles of the liquid bridge at 4 different distances L : the two separated droplets are at $L = 22$, the “in-bridge” is at $L = 17$, the cylindrical bridge is at $L = 9, 5$ and the “out-bridge” at $L = 6$. The thick dark lines indicate the lyophilic region of the substrate. Each point is obtained from averaging over 19 runs of $1.05 \cdot 10^6$ MD steps, while the data points around the minimum ($6.5 < L < 8.5$) are averaged over 29 runs. The arrow at $L = 22$ indicates that bridges are no longer stable for $L \geq 22$. The contact angle at zero force is $\theta^* \approx 100^\circ$.

FIG. 8. Midheight radius $R(Z = L/2, t)$ of a forming liquid bridge as a function of time, for $L = 21.5$. The radial distance from the vertical axis of the droplet to the point where the density is $\rho = 1.0$

is measured. The origin of time $t = 0$ is chosen as the time when the two droplets sitting on opposite parallel substrates have just touched each other. The insets show vertical cross sections of the resulting bridges for three different times indicated in the figure. $R(Z = L/2, t)$ is averaged over 7 independent runs. For $300 \leq t \leq 3000$ an effective growth law $R(Z = L/2, t) \propto \text{const} + t^{0.242}$ is observed, as indicated by a straight line.

FIG. 9. Density profiles of a forming liquid bridge for four different times, as indicated in the figure. The diffusive interpenetration of species which originally belong to the two separated droplets is indicated.

-
1. R. Wang et al., Nature **388**, 431 (1998)
 2. G. Möller, M. Hake, and H. Motschmann, Langmuir **14**, 4955 (1998)
 3. G. P. Lopez, H. A. Biebuyck, C. D. Frisbie, and G. M. Whitesides, Science **260**, 647 (1993)
 4. J. Drelich, J. D. Miller, A. Kumar, and G. M. Whitesides, Colloids Surf. A **93**,1 (1994)
 5. F. Morhard, J. Schumacher, A. Lenenbach, T. Wilhelm, R. Dahint, M. Grunze, and D. S. Everhart, Electrochem. Soc. Proc. **97**, 1058 (1997)
 6. H. Gau, S. Herminghaus, P. Lenz, and R. Lipowsky, Science **283**, 46 (1999)
 7. R. Wang, A. N. Parckh, J. D. Beers, A. P. Shreve, and B. Swanson, J. Phys. Chem. B **103**, 10149 (1999)
 8. M. Gleiche, L. F. Chi, and H. Fuchs, Nature **403**, 173 (2000)
 9. R. C. Hayward, D. A. Saville, and I. A. Aksay, Nature **404**, 173 (2000)
 10. F. Burmeister, C. Schäfer, T. Matthews, M. Böhmisch, J. Boneberg, and P. Leiderer, Langmuir **13**, 2983 (1997)
 11. J. Heier, E. J. Kramer, S. Walheim, and G. Krausch, Macromolecules **30**, 6610 (1997)
 12. P. Lenz and R. Lipowsky, Phys. Rev. Lett. **80**, 1920 (1998)
 13. R. Lipowsky, P. Lenz and P. S. Swain, Colloids Surf. A **61**, 3 (2000)
 14. P. S. Swain and R. Lipowsky, Europhys. Lett. **43**, 209 (2000)
 15. A. Valencia, M. Brinkmann, and R. Lipowsky, Langmuir **17**, 3390 (2001)
 16. R. Lipowsky, Interface Science **9**, 105 (2001)
 17. R. Lipowsky, Curr. Opin. Colloid Interface Sci. **6**, 40 (2001)
 18. M. Brinkmann and R. Lipowsky, J. Appl. Phys. **92**, 4296 (2002)
 19. E. J. De Souza, "Capillary forces between structured substrates", Thesis, Max-Planck Institut für Metallforschung, Stuttgart, 2004.
 20. J. L. Parker, P. M. Claesson and P. Allard, J. Phys. Chem. **98**, 8468 (1994)
 21. P. Attard and S. J. Miklavcic, Langmuir **17**, 8217 (2001); P. Attard, Langmuir **12**, 1693 (1996)
 22. O. I. Vinogradova, G. E. Yakubov, and H.-J. Butt, J. Chem. Phys. **114**, 8124 (2001)
 23. D. Andrienko, P. Patricio and O. I. Vinogradova, J. Chem. Phys. (2004, in press)
 24. T. Young, Phil. Trans. R. Soc. London **5**, 65 (1805)
 25. J. S. Rowlinson and B. Widom, *Molecular Theory of Capillarity* (Clarendon, Oxford, 1982)
 26. P. G. de Gennes, Rev. Mod. Phys. **57**, 825 (1985)
 27. M. V. Berry, J. Phys. A **7**, 231 (1985)
 28. B. A. Pethica, J. Colloid Interface Sci. **62**, 569 (1977)
 29. P. Tarazona and G. Navascués, J. Chem. Phys. **75**, 2441 (1981)
 30. B. V. Toshev, D. Platikanov, and A. Scheludko, Langmuir **4**, 489 (1988)
 31. I. Szleifer and B. Widom, Mol. Phys. **75**, 925 (1992)
 32. C. Varea and A. Robledo, Physica A **183**, 121 (1992)
 33. J. Drelich, Colloids Surf. A **116**, 43 (1996)
 34. T. Getta and S. Dietrich, Phys. Rev. E **57**, 655 (1998)
 35. C. Bauer and S. Dietrich, Eur. Phys. J. B **10**, 767 (1999)
 36. F. Bresme and N. Quirke, Phys. Rev. Lett. **80**, 3791 (1998)
 37. A. Milchev and K. Binder, J. Chem. Phys. **114**, 8610 (2001)
 38. A. Milchev and K. Binder, J. Chem. Phys. **116**, 7691 (2002)
 39. J. Yaneva, A. Milchev and K. Binder, Macromol. Theory Simul. **12**, 573 (2003)
 40. F. Varnik and K. Binder, J. Chem. Phys. **117**, 6336 (2002)
 41. I. Gerroff, A. Milchev, W. Paul and K. Binder, J. Chem. Phys. **98**, 6526 (1993)
 42. A. Milchev, W. Paul and K. Binder, J. Chem. Phys. **99**, 4786 (1993)
 43. A. Milchev and K. Binder, Macromol. Theory Simul. **3**, 915 (1994)
 44. A. Milchev and K. Binder, Macromolecules **29**, 343 (1996)
 45. A. Milchev and K. Binder, J. Phys. II **6**, 21 (1996); Eur. Phys. J. B **3**, 477 (1998)
 46. R. B. Pandey, A. Milchev and K. Binder, Macromolecules **30**, 1194 (1997)
 47. A. Milchev and K. Binder, J. Chem. Phys. **106**, 1978 (1997)
 48. J. M. Thijssen, *Computational Physics* Cambridge Univ. Press, Cambridge (1999).
 49. O. M. Braun and M. Peyrard, Phys. Rev. E **63**, 046110(2001).
 50. M. Voue, M. P. Valignat, G. Oshanin, A. M. Cazabat, and J. De Coninck, Langmuir **14**, 5951 (1998)
 51. A. Arbe, M. Monkenbusch, J. Stellbrink, D. Richter, B. Farago, and R. Faust, Macromolecules **34**, 1281 (2001)
 52. A. I. Milchev and A. A. Milchev, Europhys. Lett. **56**, 695 (2001)
 53. F. Varnik, J. Baschnagel, and K. Binder, J. Chem. Phys. **113**, 4444 (2000)
 54. S. Puri and K. Binder, Phys. Rev. B **44**, 9735 (1991)

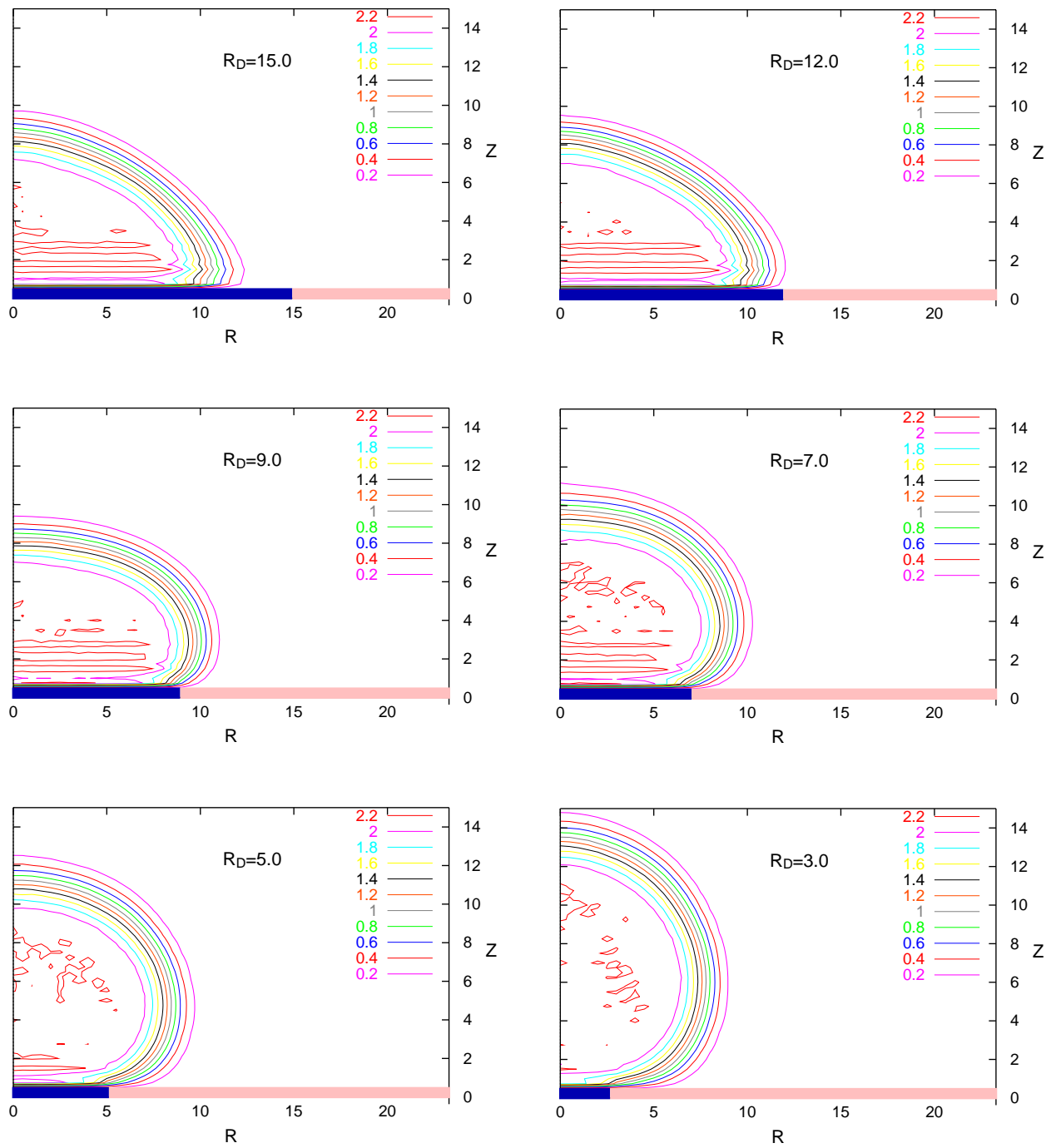


Fig. 1.

Fig. 2.

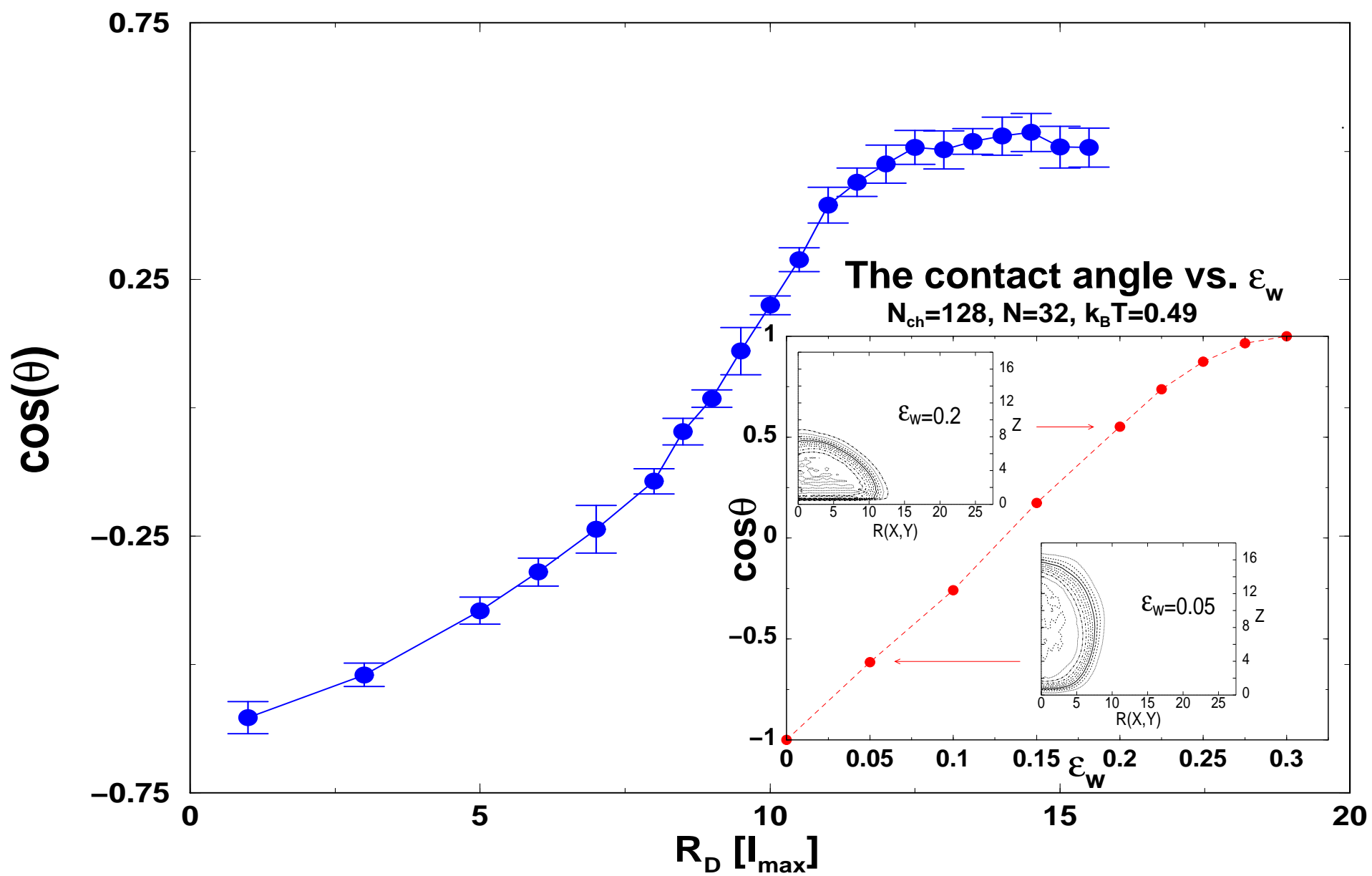
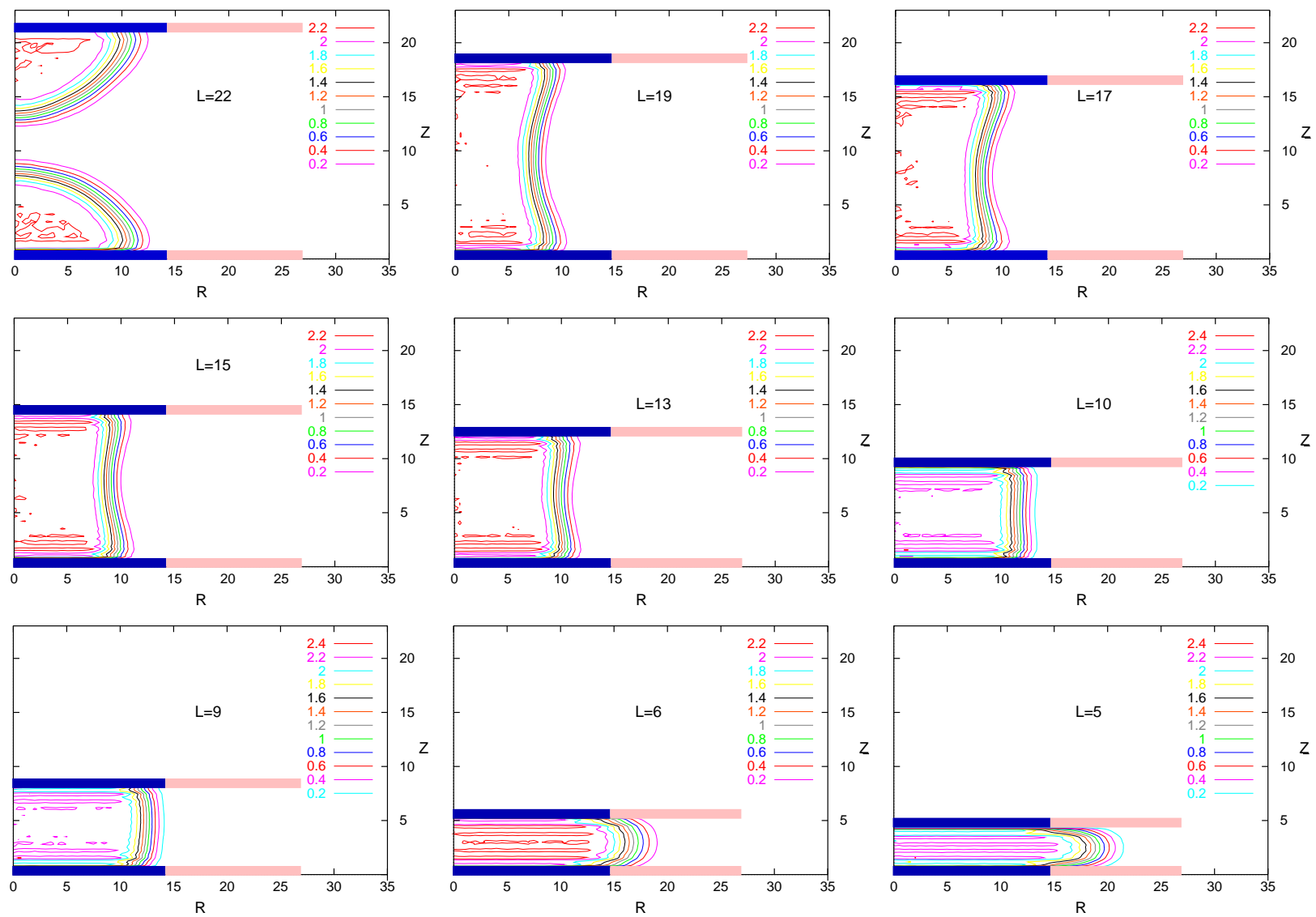


Fig. 3.



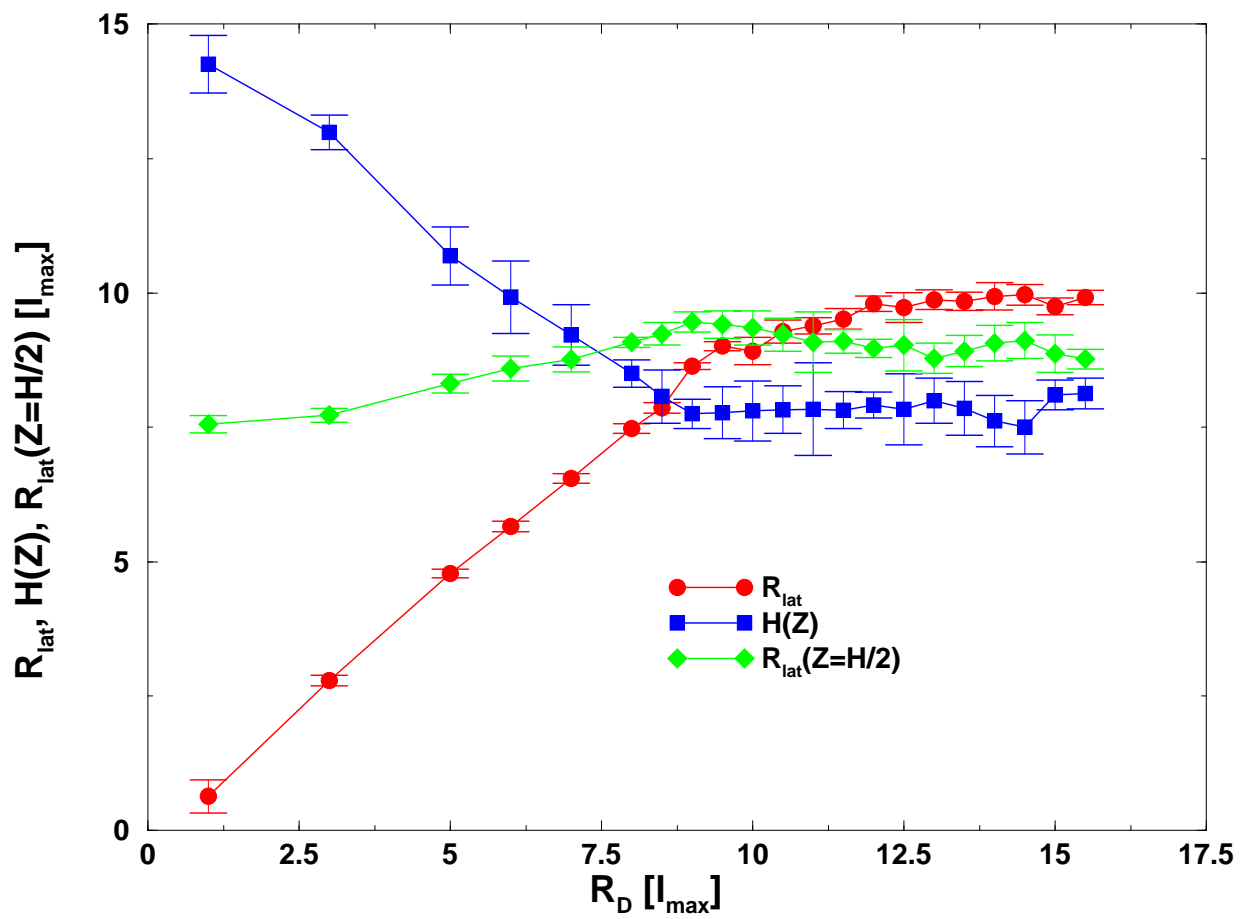


Fig. 4.

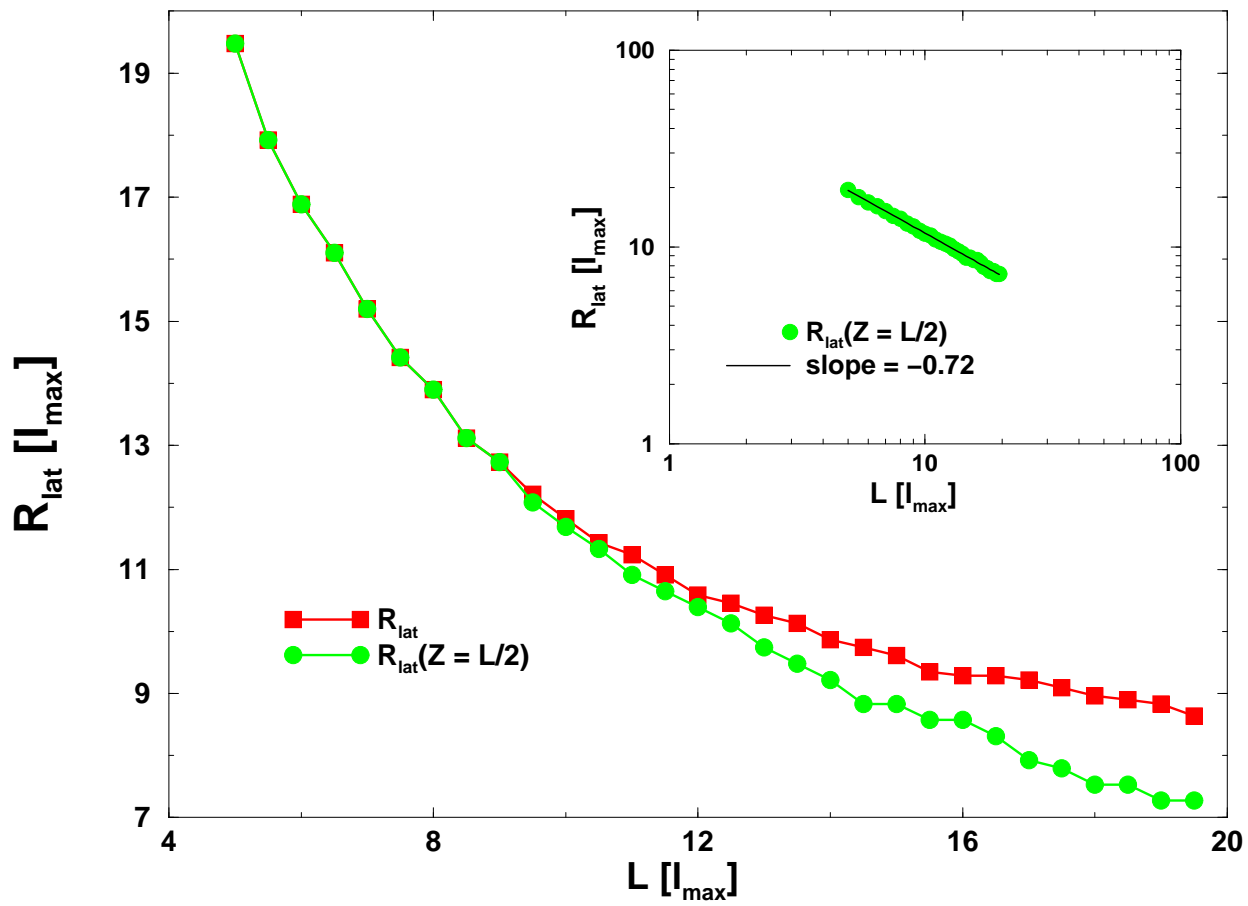


Fig. 5.

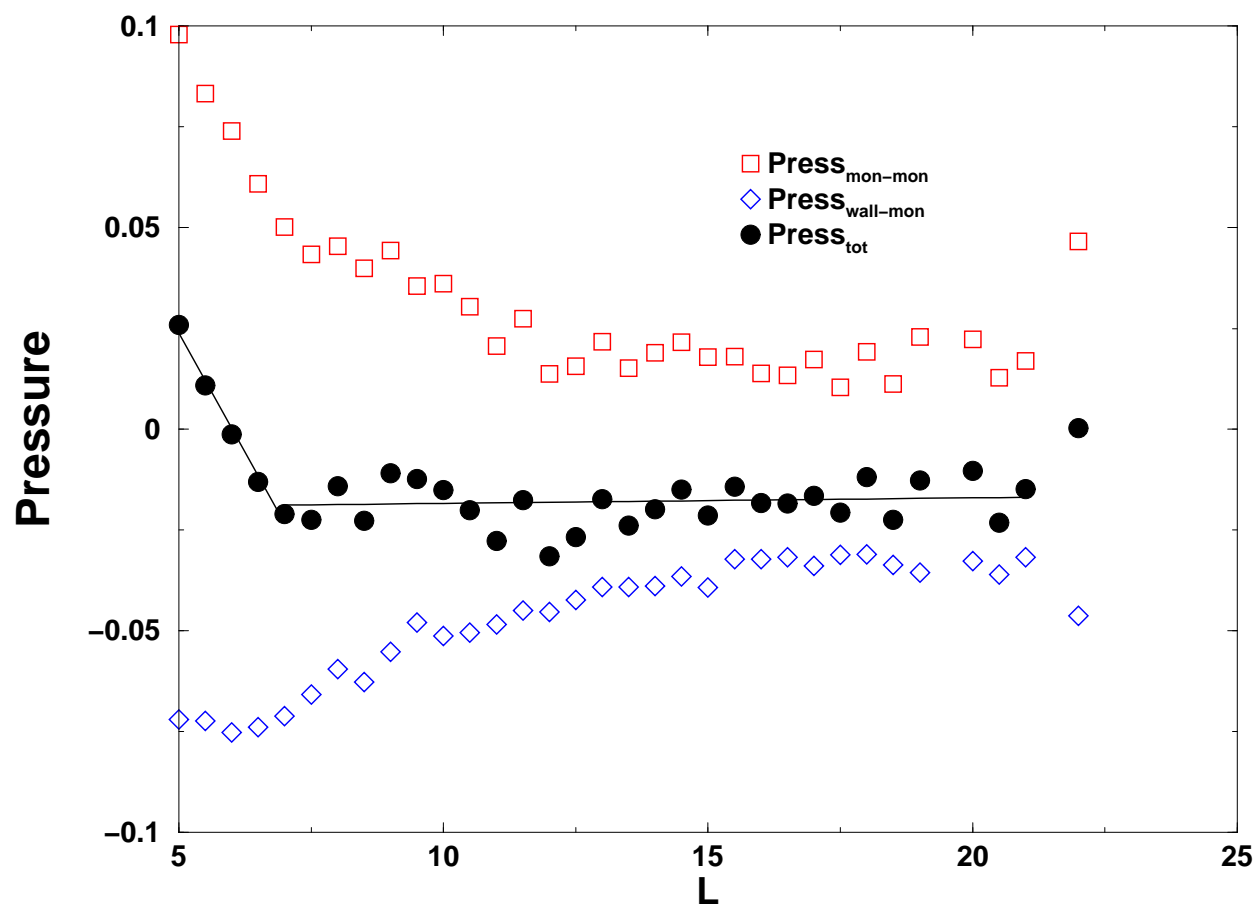


Fig. 6.

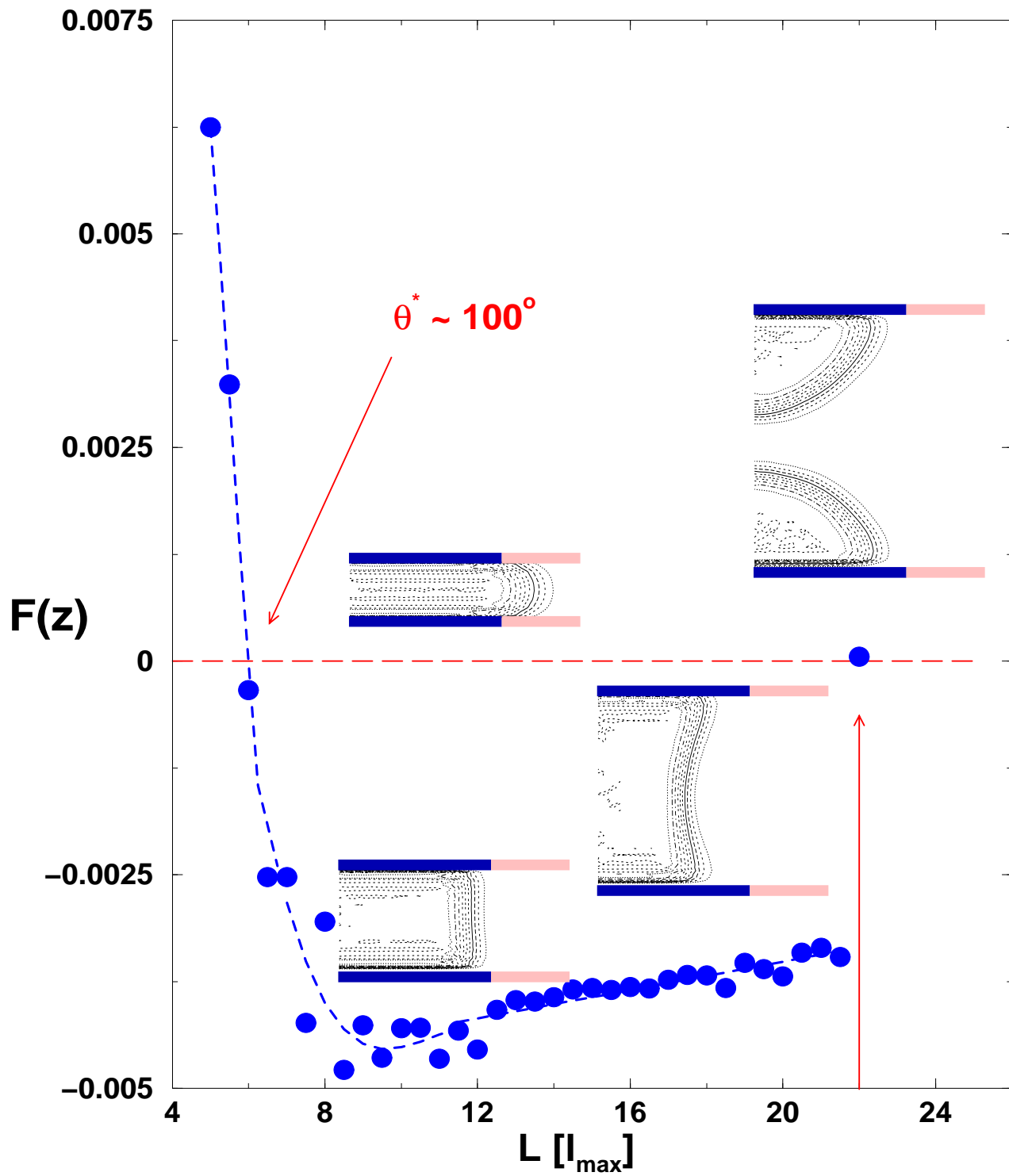


Fig. 7.

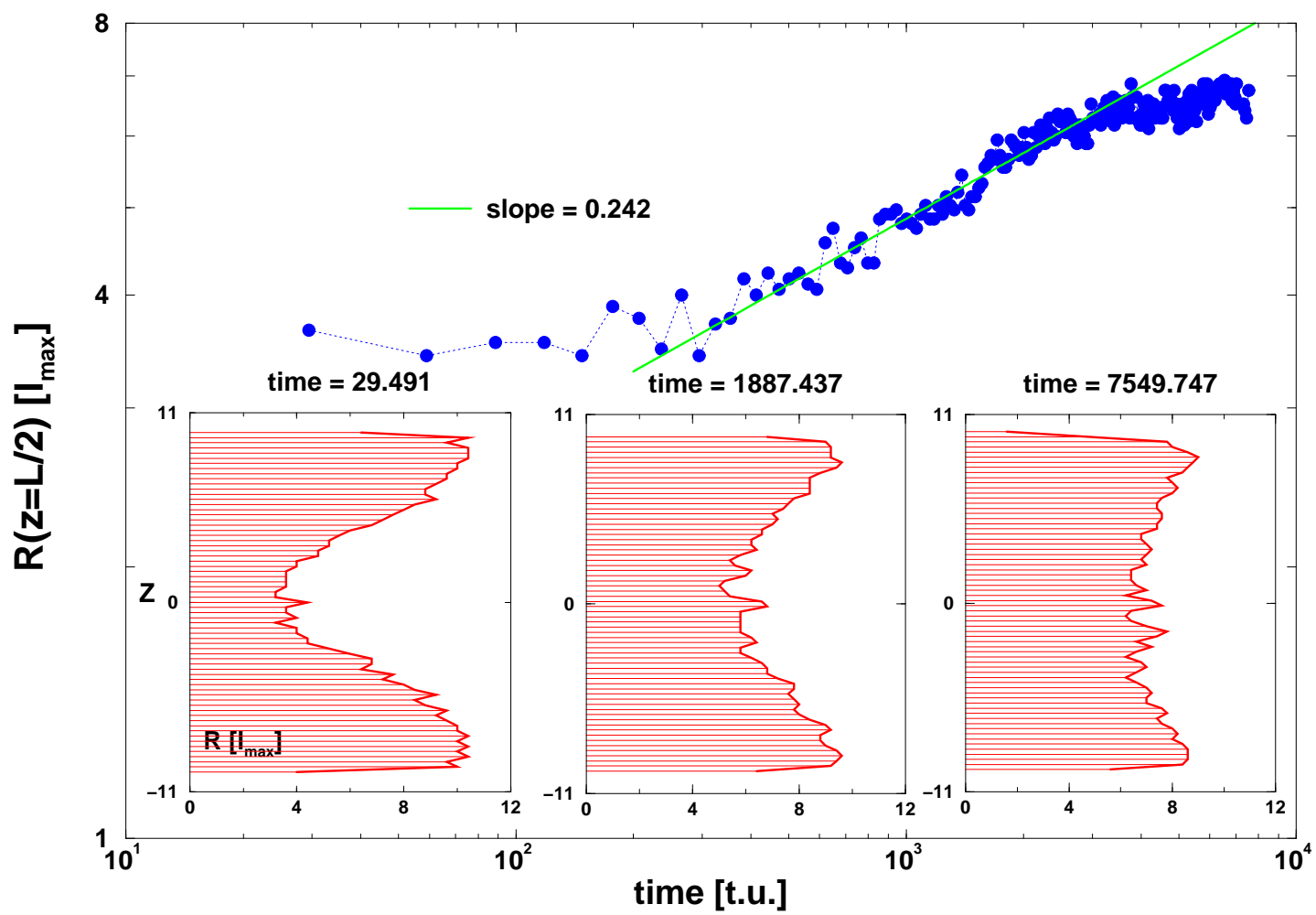


Fig. 8.

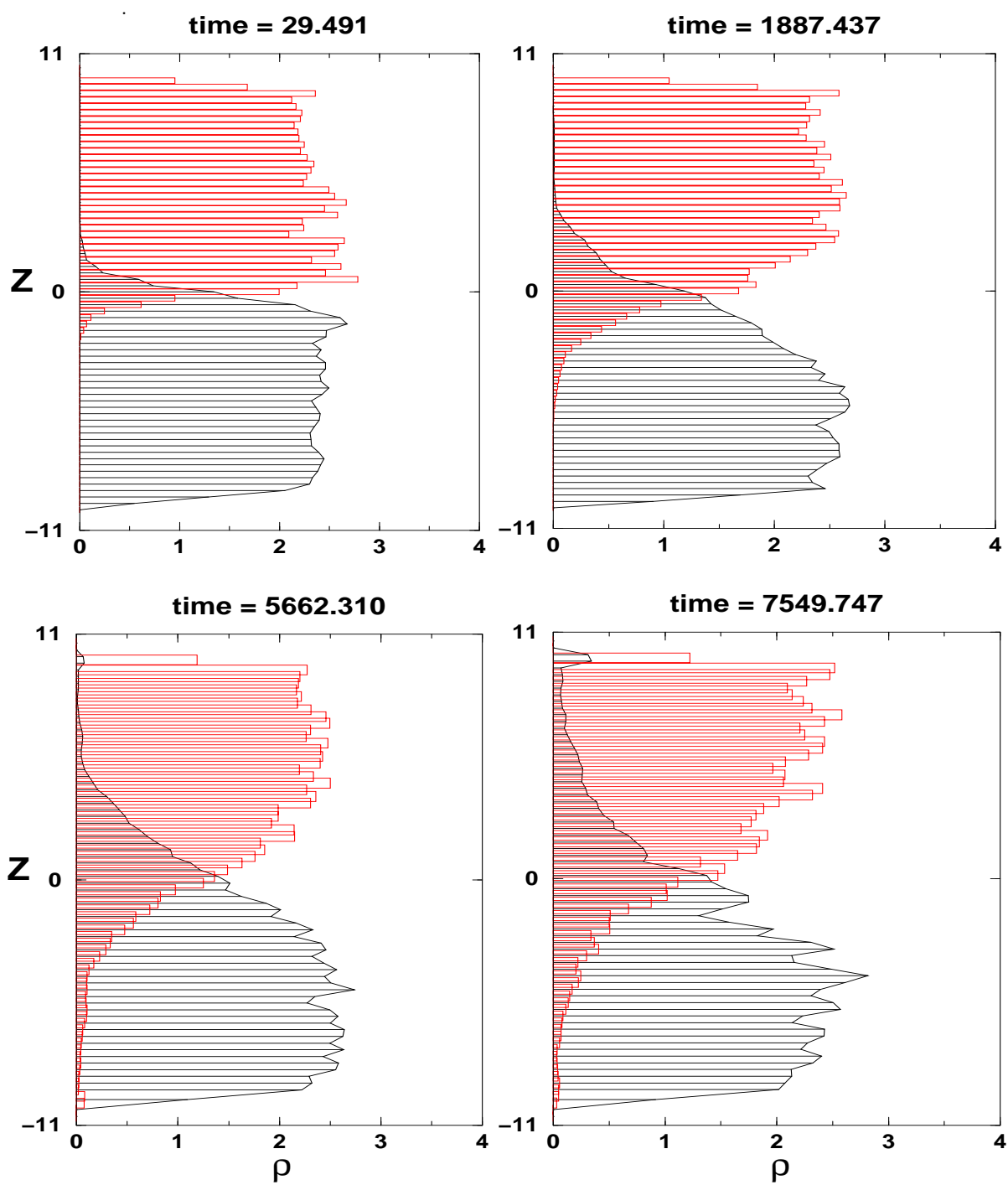


Fig. 9.